Turbulent Channel and Couette Flows Using an Anisotropic k-ϵ Model

Shoiti Nisizima* and Akira Yoshizawa†
University of Tokyo, Tokyo, Japan

Turbulent channel and Couette flows are studied numerically by using an anisotropic k-ϵ model. A feature of this model lies in an anisotropic expression for the Reynolds stress and the deviation of the Reynolds stress from an isotropic eddy-viscosity representation is incorporated. Only one kind of wall damping function is introduced to impose the no-slip boundary condition on solid walls. The results obtained show that turbulence quantities of channel and Couette flows are in good agreement with experimental data and numerical results from large-eddy simulation. The anisotropy of turbulent intensities, which the usual k-ϵ model cannot predict, is well reproduced.

I. Introduction

WITH the recent advance of computers, the numerical study of fluid motions has made much progress. For example, we may examine numerically flows at high Reynolds numbers and the transition of laminar flows to turbulence. However, the direct simulation of turbulent flows appearing in engineering and natural sciences cannot be carried out by even the largest existing computers. This fact is entirely due to the number of scales contained in turbulent flows. Therefore, some turbulence models are indispensable for their numerical simulation.

As representative turbulence models, there exist the large-eddy simulation (LES),[1-6] stress, and k-ϵ models.[7-12] In engineering problems, the k-ϵ model based on an isotropic eddy-viscosity representation for the Reynolds stress is widely used, mainly due to short computing times and the simplicity of model. Recently, this model has been improved to treat the flow in the vicinity of solid walls by using wall damping functions.[13-17] However, owing to the intrinsic isotropic property of the k-ϵ model, the anisotropy of turbulent intensities may not be predicted accurately.

In order to overcome the difficulties of the k-ϵ model, various types of stress models have been developed. In those models, no use is made of an eddy-viscosity representation for the Reynolds stress. Therefore, the stress models can predict the strong anisotropy of turbulent intensities in the wall turbulence. In the treatment of flows with three-dimensional mean flows, however, the number of flow quantities in the stress models increases significantly compared with the k-ϵ model.

With the advent of supercomputers, LES is becoming a very promising simulation method for turbulent flows. The LES model is generally simpler than the other two types of models and is expected to be more universal. However, LES requires much finer grid resolution and much longer computing times than the stress or k-ϵ models. Therefore, stress and k-ϵ models based on the Reynolds-averaging procedure are still very important in engineering sciences.

On comparing models the k-ϵ model is suited for the analytical investigation of modeling by means of statistical theories such as the direct-interaction approximation (DIA).[18] In fact, one of the authors developed a multiscale DIA theory[19,20] for turbulent shear flows and applied it to an investigation of k-ϵ and LES model types. As a result, there appears to be a possibility that the standard isotropic k-ϵ model may be much improved with the aid of turbulence theories.

In this paper, we propose an anisotropic k-ϵ model based on statistical results. A main feature of this model is the use of an anisotropic expression[19] for the Reynolds stress. In order to impose the no-slip condition on solid walls, only one kind of wall damping function is introduced. This anisotropic model is applied to turbulent channel and Couette flows. Comparison of the present results with experimental data and other numerical results using LES shows good agreement even in the vicinity of walls. The anisotropy of turbulent intensities, which the usual isotropic k-ϵ model cannot predict, is well reproduced.

II. Standard Isotropic k-ϵ Model

In what follows, the ensemble mean parts of the velocity and the pressure divided by fluid density are denoted by $\bar{v}$ and $\bar{p}$, respectively, and their fluctuations by v' and p', respectively. Then, the mean equations for three-dimensional incompressible flows are given by

$$\frac{\mathrm{D}\bar{v}_\alpha}{\mathrm{D}t} \equiv \left(\frac{\partial}{\partial t} + \bar{v}_a \frac{\partial}{\partial x_a}\right)\bar{v}_\alpha = -\frac{\partial \bar{p}}{\partial x_\alpha} + \frac{\partial}{\partial x_a}\left(R_{\alpha a} + \nu \frac{\partial \bar{v}_\alpha}{\partial x_a}\right) \tag{1}$$

$$\frac{\partial \bar{v}_a}{\partial x_a} = 0 \tag{2}$$

where ν is the kinematic viscosity, $R_{\alpha\beta}$ the Reynolds stress defined as

$$R_{\alpha\beta} = -\langle v'_\alpha v'_\beta \rangle \tag{3}$$

by using the ensemble mean $\langle\ \rangle$, and repeated roman subscripts are summed from 1 to 3 (for clarity, Greek letters are used for noncontracted subscripts).

In the standard isotropic k-ϵ model,[11] $R_{\alpha\beta}$ is approximated by using the eddy viscosity ν_e as

$$R_{\alpha\beta} = -\tfrac{2}{3}k\delta_{\alpha\beta} + \nu_e e_{\alpha\beta} \tag{4}$$

where k is the turbulent kinetic energy, $\delta_{\alpha\beta}$ the Kronecker delta symbol, and $e_{\alpha\beta}$ the velocity strain defined by

$$e_{\alpha\beta} = \frac{\partial \bar{v}_\alpha}{\partial x_\beta} + \frac{\partial \bar{v}_\beta}{\partial x_\alpha} \tag{5}$$

Received March 10, 1986; revision received July 14, 1986,

*Associate Research Fellow, Institute of Industrial Science.
†Associate Professor, Institute of Industrial Science.

From dimensional analysis, ν_e is written as

$$\nu_e = C_\nu \frac{k^2}{\epsilon} \tag{6}$$

in terms of k and the dissipation rate ϵ of the turbulent kinetic energy (C_ν is a model constant). The governing equations for k and ϵ are modeled in the form that

$$\frac{Dk}{Dt} = R_{ab}\frac{\partial \bar{v}_b}{\partial x_a} - \varepsilon + \frac{\partial}{\partial x_a}\left(C_k \frac{k^2}{\epsilon}\frac{\partial k}{\partial x_a} + \nu \frac{\partial k}{\partial x_a}\right) \tag{7}$$

$$\frac{D\epsilon}{Dt} = \frac{1}{2}C_{\epsilon 1} k e_{ab} e_{ab} - C_{\epsilon 2}\frac{\varepsilon^2}{k} + \frac{\partial}{\partial x_a}\left(C_{\epsilon 3}\frac{k^2}{\epsilon}\frac{\partial \epsilon}{\partial x_a} + \nu \frac{\partial \epsilon}{\partial x_a}\right) \tag{8}$$

where C_k, $C_{\epsilon 1}$, etc., are model constants. Thus, Eqs. (1), (2), and (4-8) constitute a closed system of equations. The model constants are usually chosen as[11]

$$C_\nu \sim 0.09,\ C_k \sim 0.09,\ C_{\epsilon 1} \sim 0.13,\ C_{\epsilon 2} \sim 1.9,\ C_{\epsilon 3} \sim 0.069 \tag{9}$$

The modeling of the k-ϵ type shown above cannot be applied to analyses in the vicinity of solid walls. Recently, many devices for imposing the no-slip boundary condition on the walls have been developed to resolve this difficulty. As such representatives, we may mention the introduction of some kinds of wall damping functions into the modeling-related terms in Eqs. (1), (7), and (8).[13-17] Similar devices are also made in LES of channel flows.[4,6]

III. Anisotropic k-ϵ Model

Equation (4) for $R_{\alpha\beta}$ cannot predict the anisotropy of turbulent intensities. For example, in the turbulent channel flows examined in this paper (Fig. 1a), we have

$$\bar{v}_2 = \bar{v}_3 = 0, \qquad \frac{\partial \bar{v}_1}{\partial x_1} = \frac{\partial \bar{v}_1}{\partial x_3} = 0 \tag{10}$$

Consequently, Eq. (4) leads to the isotropy of turbulent intensities; namely, we have

$$\langle v_1'^2\rangle = \langle v_2'^2\rangle = \langle v_3'^2\rangle = \tfrac{2}{3}k \tag{11}$$

This fact contradicts the experimental data.

Recently, a more elaborate expression for $R_{\alpha\beta}$ has been found statistically by using a multiscale DIA theory.[19] It may be expressed in the form

$$R_{\alpha\beta} = -\frac{2}{3}k\delta_{\alpha\beta} + \nu_e\left(\frac{\partial \bar{v}_\alpha}{\partial x_\beta} + \frac{\partial \bar{v}_\beta}{\partial x_\alpha}\right) + \frac{1}{3}\left(\sum_{m=1}^{3}\tau_m S_{maa}\right)\delta_{\alpha\beta} + R'_{\alpha\beta} \tag{12}$$

where ν_e has been given by Eq. (6) and

$$\tau_m = C_{\tau m}\frac{k^3}{\epsilon^2} \tag{13}$$

$$S_{1\alpha\beta} = \frac{\partial \bar{v}_\alpha}{\partial x_a}\frac{\partial \bar{v}_\beta}{\partial x_a} \tag{14}$$

$$S_{2\alpha\beta} = \frac{1}{2}\left(\frac{\partial \bar{v}_\alpha}{\partial x_a}\frac{\partial \bar{v}_a}{\partial x_\beta} + \frac{\partial \bar{v}_\beta}{\partial x_a}\frac{\partial \bar{v}_a}{\partial x_\alpha}\right) \tag{15}$$

$$S_{3\alpha\beta} = \frac{\partial \bar{v}_a}{\partial x_\alpha}\frac{\partial \bar{v}_a}{\partial x_\beta} \tag{16}$$

$$R'_{\alpha\beta} = -\sum_{m=1}^{3}\tau_m S_{m\alpha\beta} \tag{17}$$

and $C_{\tau m}$ ($m = 1,2,3$) are model constants. The first two terms on the right-hand side of Eq. (12) give the familiar isotropic eddy-viscosity representation. On the other hand, the third and fourth terms are crucially important in expressing the anisotropy of $R_{\alpha\beta}$. In reality, the turbulent intensities in channel flows are given as

$$\langle v_1'^2\rangle = \frac{2}{3}k + \frac{1}{3}(2C_{\tau 1} - C_{\tau 3})\frac{k^3}{\epsilon^2}\left(\frac{\partial \bar{v}_1}{\partial x_2}\right)^2 \tag{18}$$

$$\langle v_2'^2\rangle = \frac{2}{3}k - \frac{1}{3}(C_{\tau 1} - 2C_{\tau 3})\frac{k^3}{\epsilon^2}\left(\frac{\partial \bar{v}_1}{\partial x_2}\right)^2 \tag{19}$$

$$\langle v_3'^2\rangle = \frac{2}{3}k - \frac{1}{3}(C_{\tau 1} + C_{\tau 3})\frac{k^3}{\epsilon^2}\left(\frac{\partial \bar{v}_1}{\partial x_2}\right)^2 \tag{20}$$

which leads to the anisotropy of the turbulent intensities encountered in channel flows. It should be noted here that one model constant ($C_{\tau 2}$) does not appear in one-dimensional channel and Couette flows. Two other constants ($C_{\tau 1}$ and $C_{\tau 3}$) are chosen so that the computed results reproduce the observed anisotropy of the turbulent intensities in channel flow as accurately as possible. We adopt

$$C_{\tau 1} = 0.07, \qquad C_{\tau 3} = -0.015 \tag{21}$$

in the present paper. Optimization of the remaining constant $C_{\tau 2}$ is left for future work.

Here, we should note that those anisotropic terms do not contribute to the shear stress in the case of one-dimensional channel and Couette flows. In reality, we have

$$-\langle v_1' v_2'\rangle = \nu_e \frac{\partial \bar{v}_1}{\partial x_2} \tag{22}$$

Therefore, the mean velocity $\bar{v}_1$, the turbulent kinetic energy k, and the energy dissipation rate ϵ are not influenced by such anisotropy.

In what follows, Eq. (12) with Eq. (13-17) and (21) is incorporated into the k-ϵ modeling. Hereafter, we call this model the anisotropic k-ϵ model.

IV. Numerical Method in Channel Flows

Fundamental Equations

In the fully developed channel flows depicted in Fig. 1a, we have

$$\frac{\partial \bar{v}_1}{\partial x_1} = 0,\ \bar{v}_2 = \bar{v}_3 = 0$$

$$\frac{\partial \bar{p}}{\partial x_1} = \text{const},\ \frac{\partial \bar{p}}{\partial x_2} = \frac{\partial \bar{p}}{\partial x_3} = 0 \tag{23}$$

We nondimensionalize x_2, $\bar{v}_1$, k, and ϵ by using the characteristic (or equivalently, friction) velocity $\sqrt{-(d\bar{p}/dx_1)D}$ and the half-width of channel D. Then, the fundamental equations (1), (7), and (8) are reduced to

$$\frac{\partial \bar{v}_1}{\partial t} = 1 + \frac{\partial}{\partial x_2}\left(C_\nu \frac{k^2}{\epsilon}\frac{\partial \bar{v}_1}{\partial x_2} + \frac{1}{R}\frac{\partial \bar{v}_1}{\partial x_2}\right) \tag{24}$$

$$\frac{\partial k}{\partial t} = C_\nu \frac{k^2}{\epsilon}\left(\frac{\partial \bar{v}_1}{\partial x_2}\right)^2 - \epsilon + \frac{\partial}{\partial x_2}\left(C_k \frac{k^2}{\epsilon}\frac{\partial k}{\partial x_2} + \frac{1}{R}\frac{\partial k}{\partial x_2}\right) \tag{25}$$

$$\frac{\partial \epsilon}{\partial t} = C_{\epsilon 1} k \left(\frac{\partial \bar{v}_1}{\partial x_2} \right)^2 - C_{\epsilon 2} \frac{\epsilon^2}{k} + \frac{\partial}{\partial x_2} \left(C_{\epsilon 3} \frac{k^2}{\epsilon} \frac{\partial \epsilon}{\partial x_2} + \frac{1}{R} \frac{\partial \epsilon}{\partial x_2} \right) \tag{26}$$

where the Reynolds number R is defined by

$$R = \frac{D}{\nu} \sqrt{D \left(- \frac{\mathrm{d} \bar{p}}{\mathrm{d} x_1} \right)} \tag{27}$$

In what follows, we shall also use another Reynolds number R_c based on the centerline velocity and the half-width of the channel.

Neither the isotropic eddy-viscosity representation [Eqs. (4) and (6)] nor the present anisotropic one [Eqs. (12-17)] holds in the close vicinity of solid walls, where the effect of viscosity ν plays an essential role. As in a number of previous works,[13-17] we also introduce a wall damping function to remove the difficulty. At this time, it is desirable to make the number of wall damping functions as small as possible. In the present work, we use only one wall damping function given by

$$f_d = 1 - \exp(-y^+/A), \quad A = 5.2 \tag{28}$$

where y^+ is the distance from a wall in wall units.

By multiplying the modeling-related terms in Eqs. (24-26) by f_d of Eq. (28), we get

$$\frac{\partial \bar{v}_1}{\partial t} = 1 + \frac{\partial}{\partial x_2} \left(f_d C_\nu \frac{k^2}{\epsilon} \frac{\partial \bar{v}_1}{\partial x_2} + \frac{1}{R} \frac{\partial \bar{v}_1}{\partial x_2} \right) \tag{29}$$

$$\frac{\partial k}{\partial t} = f_d C_\nu \frac{k^2}{\epsilon} \left(\frac{\partial \bar{v}_1}{\partial x_2} \right)^2 - \epsilon + \frac{\partial}{\partial x_2} \left(C_k f_d \frac{k^2}{\epsilon} \frac{\partial k}{\partial x_2} + \frac{1}{R} \frac{\partial k}{\partial x_2} \right) \tag{30}$$

$$\frac{\partial \epsilon}{\partial t} = C_{\epsilon 1} k \left(\frac{\partial \bar{v}_1}{\partial x_2} \right)^2 - C_{\epsilon 2} f_d^2 \frac{\epsilon^2}{k} + \frac{\partial}{\partial x_2} \times \left(C_{\epsilon 3} f_d \frac{k^2}{\epsilon} \frac{\partial \epsilon}{\partial x_2} + \frac{1}{R} \frac{\partial \epsilon}{\partial x_2} \right) \tag{31}$$

Especially, we should note the second term on the right-hand side of Eq. (31), where f_d^2 is used. This multiplication is due to the fact that the corresponding term in Eq. (26) diverges in the form of $(y^+)^{-2}$ near the walls since k is proportional to $(y^+)^2$ there.

Finite-Difference Form and Boundary Conditions

On reducing Eqs. (29-31) to a finite-difference form, we adopt the second-order finite-difference form[5]

$$\left(\frac{\mathrm{d} v}{\mathrm{d} x} \right)_i = \frac{1}{x_{i+1} - x_{i-1}} \times \left[\frac{x_i - x_{i-1}}{x_{i+1} - x_i} (v_{i+1} - v_i) + \frac{x_{i+1} - x_i}{x_i - x_{i-1}} (v_i - v_{i-1}) \right] \tag{32}$$

$$\left(\frac{\mathrm{d}^2 v}{\mathrm{d} x^2} \right)_i = 2 \left[\frac{v_{i-1}}{(x_{i+1} - x_{i-1})(x_i - x_{i-1})} - \frac{v_i}{(x_i - x_{i-1})(x_{i+1} - x_i)} + \frac{v_{i+1}}{(x_{i+1} - x_i)(x_{i+1} - x_{i-1})} \right] \tag{33}$$

concerning the spatial derivatives, where i denotes the location of the ith mesh point. On the other hand, the time derivative is approximated by using an implicit scheme of the Crank-Nicolson type. Namely, the time derivative

$$\frac{\mathrm{d} v}{\mathrm{d} t} = f \tag{34}$$

is rewritten as

$$v^{n+1} = v^n + \tau \frac{f^{n+1} + f^n}{2} \tag{35}$$

where τ is the time interval and n the nth time step.

The boundary conditions on the walls are

$$\bar{v}_1 = k = 0, \qquad \epsilon = \frac{1}{R} \frac{\partial^2 k}{\partial x_2^2} \tag{36}$$

Here, the last condition is found by using Eq. (30) on the walls. Since this condition is written in the form of the second spatial derivative, it often generates numerical instability. The condition is usually replaced by[9,10]

$$\epsilon = \frac{2}{R} \left(\frac{\mathrm{d} \sqrt{k}}{\mathrm{d} x_2} \right)^2 \tag{37}$$

since k is proportional to the square of distance from the walls.

The mesh points between two walls are given by

$$x_2 = \tanh(Y) \quad (-3.1 < Y < 3.1 \text{ for } R = 600 \text{ or } R_c = 12{,}704; \; -3.5 < Y < 3.5 \text{ for } R = 1400 \text{ or } R_c = 32{,}637) \tag{38}$$

with Y divided into N mesh points in equal distance. In the present paper, we choose $N = 61$. In this grid resolution, three mesh points lie in the so-called viscous layer ($y^+ \leqq 5$) and more than half of the mesh points fall in the region $y^+ \leqq 100$. This choice of grid resolution has been made from the following requirement necessary to perform an accurate simulation:

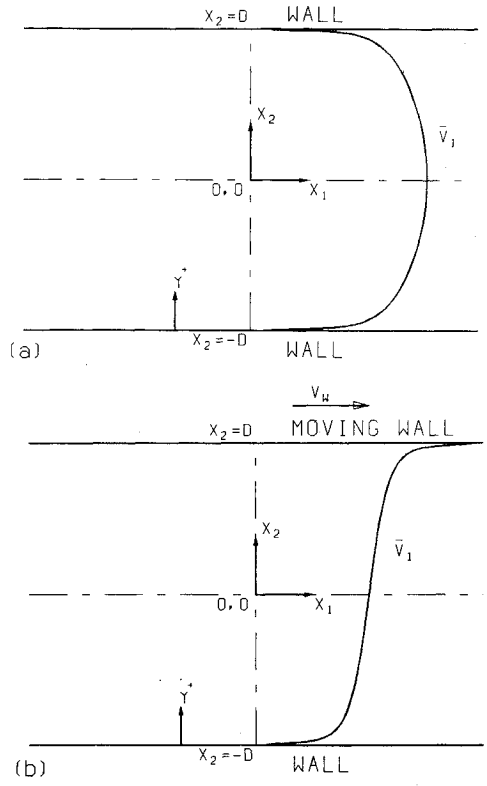

Fig. 1 Coordinate system: a) channel flow (y^+ denotes the distance from the wall in wall units); b) Couette flow.

1) the number of grid points should be large enough to resolve the rapid spatial change of flow quantities in the region $0 \leqq y^+ \leqq 100$ and 2) grid points should not be located too sparsely in the centerline region. From this requirement, the choice of $N = 31$ is not sufficient, which was also confirmed in the actual simulation. For N greater than 61, the results obtained were grid independent.

In this work, we simulate only half of the channel region owing to flow symmetry. Concerning the model constants C_k, $C_{\epsilon 1}$, $C_{\epsilon 2}$, and $C_{\epsilon 3}$, we adopt the same values as in Eq. (9) of the standard k-ϵ model. For C_ν, however, we use the somewhat larger value of

$$C_\nu = 0.094 \tag{39}$$

V. Application to Couette Flow

We further apply the present anisotropic k-ϵ model to turbulent Couette flow (Fig. 1b) with no change in the model constants or the wall damping function. In this case, we nondimensionalize $\bar{v}_1$ by the velocity V_w of a moving wall and x_2 by the half-width of channel D. Noticing that $\bar{p} = \text{const}$, Eq. (29) is replaced by

$$\frac{\partial \bar{v}_1}{\partial t} = \frac{\partial}{\partial x_2}\left(f_d C_\nu \frac{k^2}{\epsilon}\frac{\partial \bar{v}_1}{\partial x_2} + \frac{1}{R_w}\frac{\partial \bar{v}_1}{\partial x_2}\right) \tag{40}$$

where the Reynolds number R_w is defined as

$$R_w = V_w D/\nu \tag{41}$$

The remaining two equations (30) and (31) for k and ϵ are unchanged, apart from R being replaced by R_w. Further, the wall coordinate y^+ is given by

$$y^+ = x_2' v^*/\nu \tag{42}$$

by using the distance x_2' from the wall and the friction velocity v^*, which is calculated from

$$v^* = \sqrt{\nu\left(\frac{d\bar{v}_1}{dv_2}\right)_{\text{wall}}} \tag{43}$$

The boundary conditions are

$$\bar{v}_1 = 1, \qquad k = 0, \qquad \epsilon = 2\nu\left(\frac{d\sqrt{k}}{dx_2}\right)^2 \tag{44}$$

on the moving wall and the first part of Eq. (44) is replaced by

$$\bar{v}_1 = 0 \tag{45}$$

on the wall at rest. The mesh points are given by

$$x_2 = \tanh(Y) \quad (-3.0 < Y < +3.0) \tag{46}$$

with Y divided into 61 grid points in equal distance, as was done in Sec. IV.

VI. Results and Discussions

Channel Flows

The present anisotropic k-ϵ model has been applied to two channel flows at $R = 600$ ($R_c = 12{,}704$) and $R = 1400$ ($R_c = 32{,}637$). Figures 2-8 show the results obtained as well as the comparison with representative experimental data[13,21-23] and LES results.[4]

In Fig. 2, the profile of $\bar{v}_1$ is in excellent agreement withexperimental data by Laufer.[21] Especially, the so-called log-law profile is well reproduced near the walls. Figure 3 exhibits the turbulent kinetic energy k. In order to investigate the structure of k in more detail, let us see the anisotropy of three turbulent intensities. Each of these intensities is given by Figs. 4-6. Our results show that the intensity in the streamwise direction is smaller than the corresponding data by Clark[22]

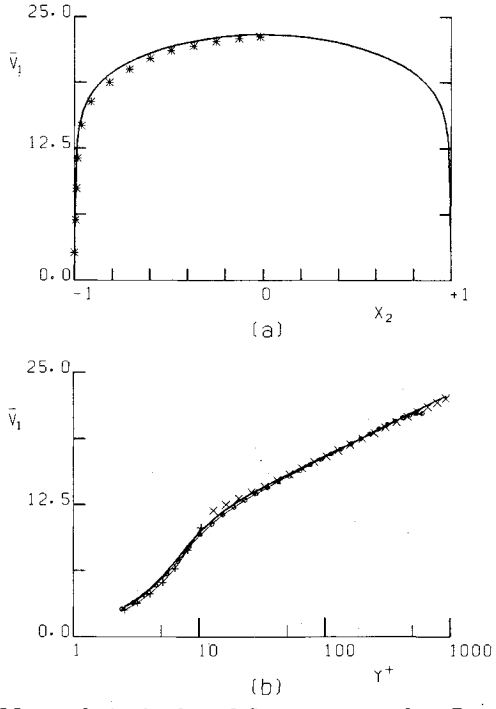

Fig. 2 Mean velocity in channel flow — computed at $R_c = 32{,}637$ and ⊖ at $R_c = 12{,}704$ vs experimental data of a) * Laufer[21] at $R_c = 30{,}800$ and b) × log-law velocity profile $[(\log y^+)/0.4 + 5.5]$ and = linear velocity profile (y^+).

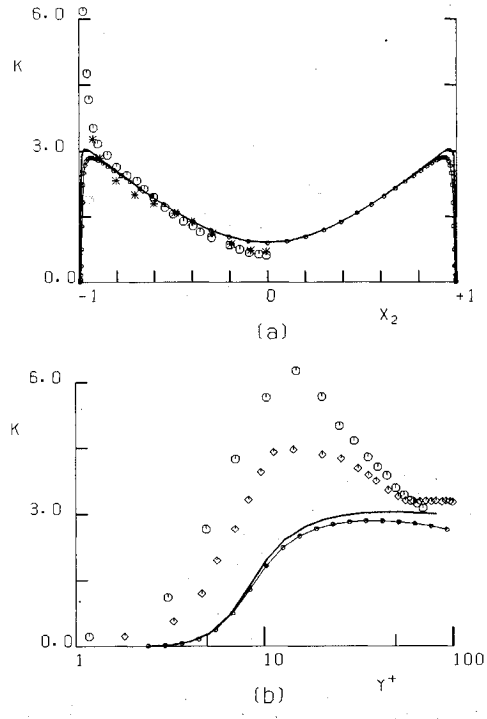

Fig. 3 Turbulent kinetic energy k in channel flow — computed at $R_c = 32{,}637$ and ⌀ at $R_c = 12{,}704$ vs experimental data of ○ Clark[22] at $R_c = 15{,}200$, of a) * Laufer[21] at $R_c = 12{,}300$, and of b) ◇ Patel et al.[13] (the average of various data around $R_c = 10{,}000$).

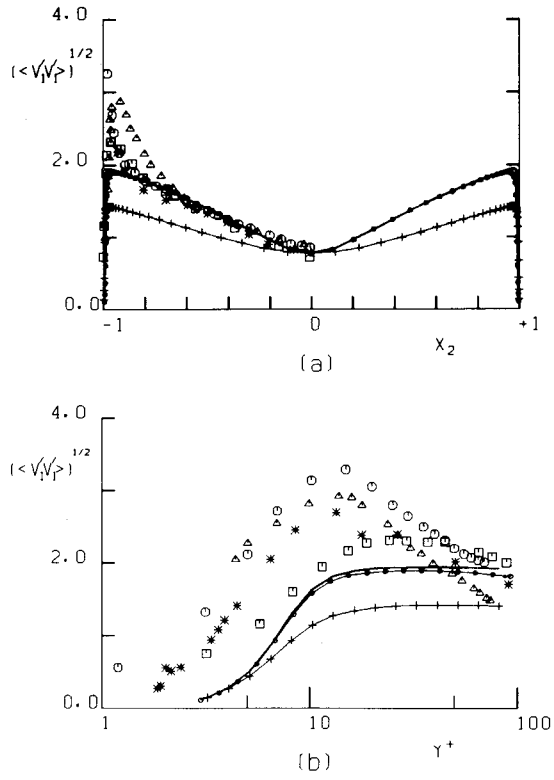

Fig. 4 $\langle v_1' v_1' \rangle^{\frac{1}{2}}$ in channel flow — computed at $R_c = 32{,}637$, ⌀ at $R_c = 12{,}704$, and by + isotropic k-ϵ model (at $R_c = 32{,}637$) vs experimental data of * Laufer[21] at $R_c = 12{,}300$, △ Kreplin and Eckelmann[23] at $R_c = 3850$, ○ Clark[22] at $R_c = 15{,}200$, and □ Moin and Kim[4] at $R_c = 13{,}800$.

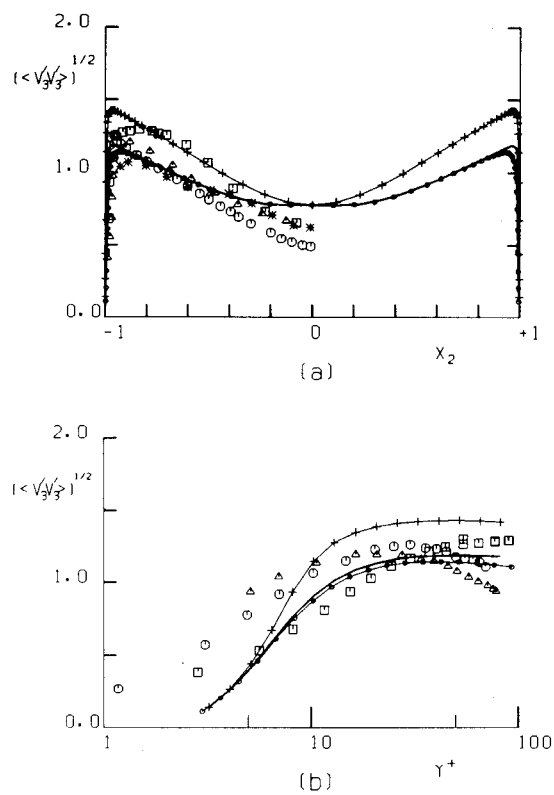

Fig. 6 $\langle v_3' v_3' \rangle^{\frac{1}{2}}$ in channel flow — computed at $R_c = 32{,}637$, ⌀ at $R_c = 12{,}704$, and by + isotropic k-ϵ model ($R_c = 32{,}637$) vs experimental data of △ Kreplin and Eckelmann[23] at $R_c = 3850$, ○ Clark[22] at $R_c = 15{,}200$, □ Moin and Kim[4] at $R_c = 13{,}800$, and * Laufer[21] at $R_c = 12{,}300$.

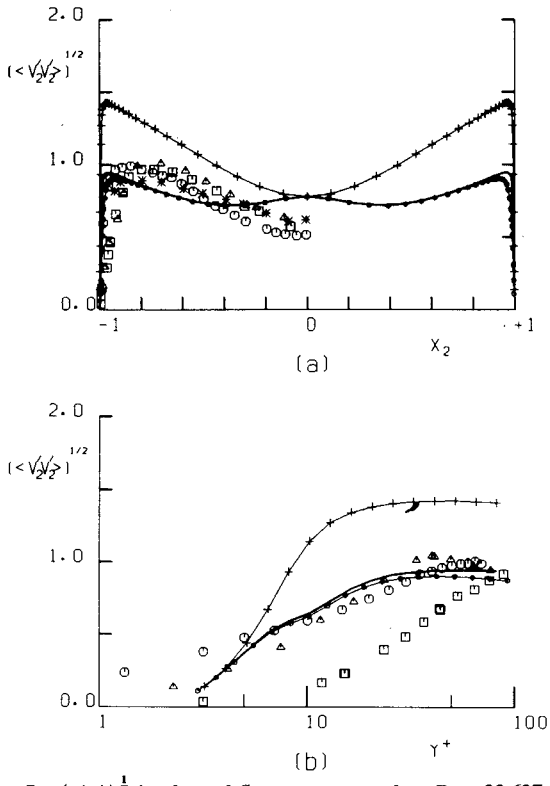

Fig. 5 $\langle v_2' v_2' \rangle^{\frac{1}{2}}$ in channel flow — computed at $R_c = 32{,}637$, ⌀ at $R_c = 12{,}704$, and by + isotropic k-ϵ model (at $R_c = 32{,}637$) vs experimental data of △ Kreplin and Eckelmann[23] at $R_c = 3850$, ○ Clark[22] at $R_c = 15{,}200$, □ Moin and Kim[4] at $R_c = 13{,}800$, * Laufer[21] at $R_c = 12{,}300$.

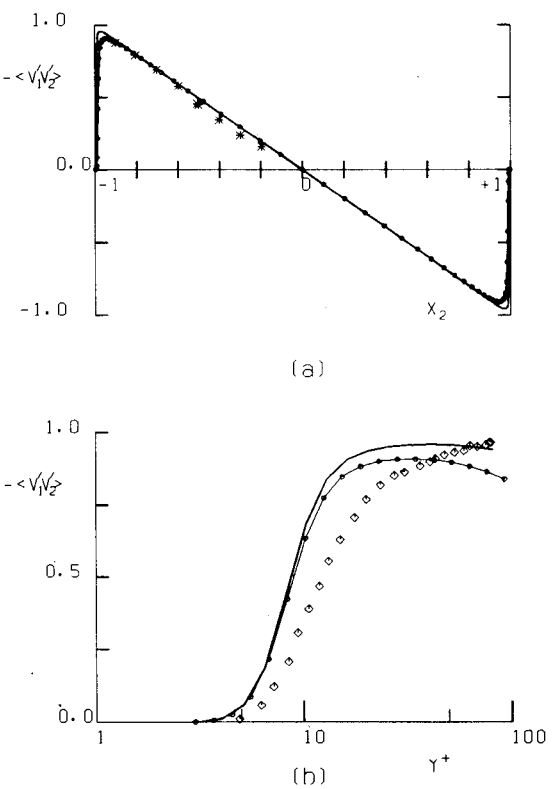

Fig. 7 Reynolds stress $-\langle v_1' v_2' \rangle$ in channel flow — computed at $R_c = 32{,}637$ and at ⊖ $R_c = 12{,}704$ vs experimental data of a) * Laufer[21] at $R_c = 30{,}800$ and b) ◇ Patel et al.[13] (the average of various data around $R_c = 10{,}000$).

and Kreplin and Eckelmann[23] (we should be careful about low Reynolds number effects in Kreplin and Eckelmann's data since their Reynolds number is rather small). This trend may be also seen in the LES results by Moin and Kim.[4] However, the overall agreement with those experimental results and the LES results by Moin and Kim is very good. Here, we should note that the anisotropy discussed here cannot be predicted at all by using the standard k-ϵ model.

Figure 7 shows the Reynolds stress; its linearity except in the close vicinity of walls is well reproduced. Figure 8 gives the dissipation rate ϵ near the wall.

Couette Flow

We next apply the present model to the Couette flow at Reynolds number $R_w = 14{,}000$ [Eq. (41)] with no change in the model constants and the wall damping function.

Figure 9 shows the mean velocity profile. Near the wall, the computed velocity profile is approximated by both linear profile and the log-law profile

$$\frac{1}{0.4}\log y^+ + A \qquad (47)$$

The constant A is usually chosen as 5.5 in channel flow, but the value is a little smaller in the present result for Couette flow. A reliable experimental value of A has not been obtained so far. The overall agreement of the present results with experiments by Robertson and Johnson[24] at $R_w = 14{,}100$ is satisfactory.

Figure 10 gives the Reynolds stress, which agrees well with a theoretical prediction by Pai[25] for very large R_w. Figures 11 and 12 show the streamwise intensity and anisotropy in three directions, respectively. The computed streamwise intensity is close to experimental data of Robertson and Johnson,[24] except near the walls. Concerning the anisotropy shown in Fig. 12, no experimental data to be compared with are available at present. On comparing Fig. 12 with Figs 4-6, we immediately notice the prominent spatial uniformity of the turbulent intensities in Couette flow.

As an interesting numerical study of Couette flows, we may mention the work of Kobayashi and Kano[26] using LES. Their result for the mean velocity agrees well with Robertson and Johnson's data,[24] but the streamwise turbulent intensity is a little smaller than the experimental data and our present result.

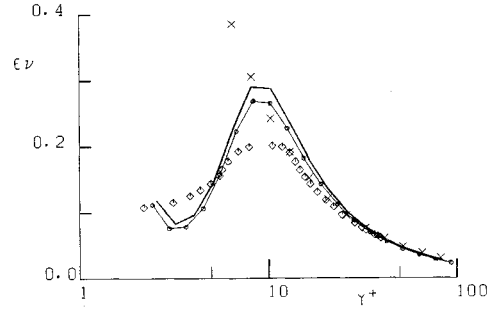

Fig. 8 Dissipation rate ϵ in channel flow — computed at $R_c = 32{,}637$ and ⌀ at $R_c = 12{,}704$ vs experimental data of ◇ Patel et al.[13] (the average of various data around $R_c = 10{,}000$); × $1/(0.4y^+)$.

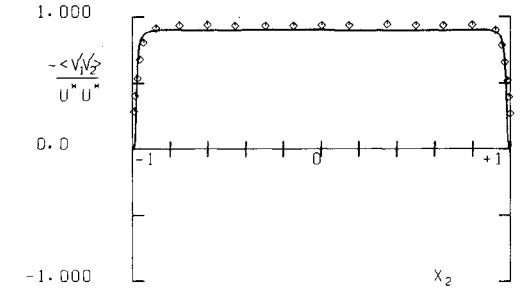

Fig. 10 Reynolds stress in Couette flow — computed at $R_w = 14{,}000$ vs ◇ Pai's theoretical prediction[25] at very large R_w.

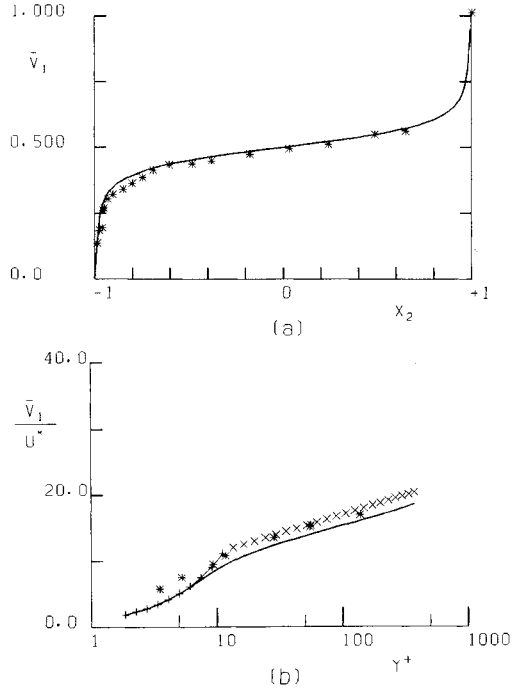

Fig. 9 Mean velocity in Couette flow — computed at $R_w = 14{,}000$ vs experimental data of * Robertson and Johnson[24] at $R_w = 14{,}100$ and × log-law profile $[(\log y^+)/0.4 + 5.5]$ and + linear velocity profile (y^+).

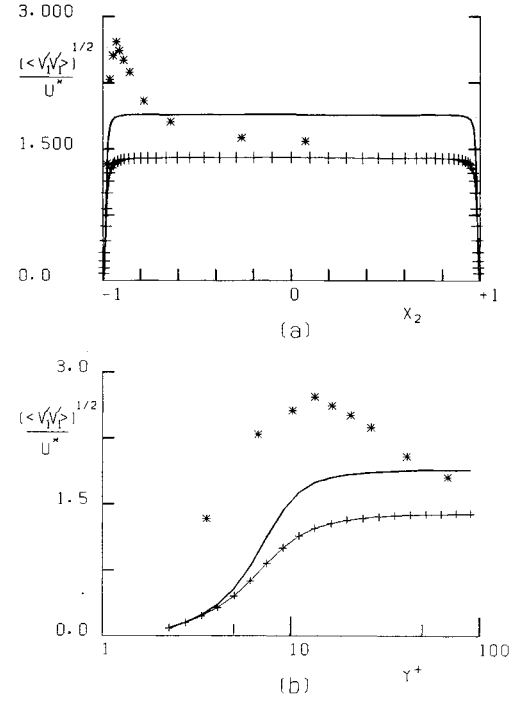

Fig. 11 $\langle v_1' v_1' \rangle^{\frac{1}{2}}/v^*$ in Couette flow — computed at $R_w = 14{,}000$ and with + isotropic k-ϵ model vs experimental data of * Robertson and Johnson[24] at $R_w = 14{,}100$.

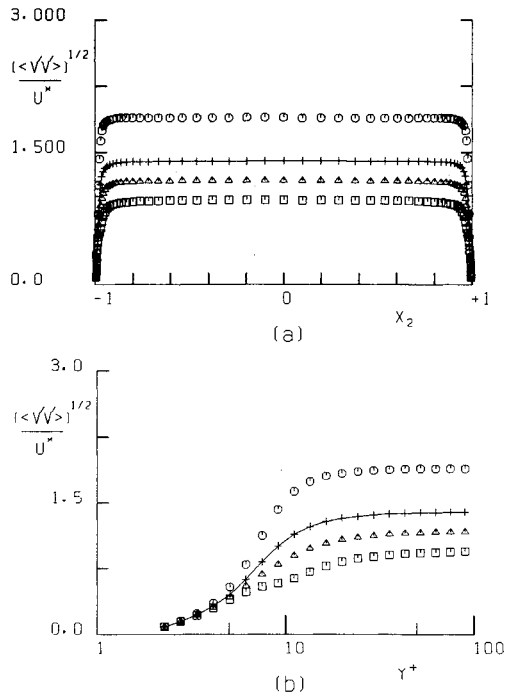

Fig. 12 Three computed turbulent intensities in Couette flow: ○ $\langle v_1'v_1'\rangle^{\frac{1}{2}}/v^*$, □ $\langle v_2'v_2'\rangle^{\frac{1}{2}}/v^*$, △ $\langle v_3'v_3'\rangle^{\frac{1}{2}}/v^*$ vs + isotropic k-ϵ model.

VII. Conclusion

In this paper, we have proposed an anisotropic k-ϵ model for the calculation of channel and Couette flows. The computed results compare satisfactorily with experimental and other numerical results. In particular, the anisotropy, which cannot be obtained by the standard k-ϵ model, is well reproduced. This improvement in the prediction of anisotropy opens up the possibility of calculating secondary flows in ducts that cannot be predicted by the standard k-ϵ model.

Acknowledgments

The authors are grateful to Dr. Kiyosi Horiuti for invaluable discussions. They are also grateful to the members of the Computer Center in Institute of Industrial Science (IIS) for useful advice and kind cooperation.

This work was partially supported by the Grant-in-Aid from IIS.

References

[1]Rogallo, R.S. and Moin, P., "Numerical Simulation of Turbulent Flows," *Annual Review of Fluid Mechanics*, Vol. 16, 1984, pp. 99-137.

[2]Deardorff, J.W., "A Numerical Study of Three-Dimensional Turbulent Channel Flow at Large Reynolds Numbers," *Journal of Fluid Mechanics*, Vol. 41, 1970, pp. 453-480.

[3]Schumann, U., "Subgrid Scale Model for Finite-Difference Simulation of Turbulent Flows in Plane Channel and Annuli," *Journal of Computational Physics*, Vol. 18, 1975, pp. 376-404.

[4]Moin, P. and Kim, J., "Numerical Investigation of Turbulent Channel Flow," *Journal of Fluid Mechanics*, Vol. 118, 1982, pp. 341-377.

[5]Horiuti, K., "Study of Incompressible Turbulent Channel Flow by Large-Eddy Simulation," *Theoretical and Applied Mechanics*, Vol. 31, 1981, pp. 407-427.

[6]Horiuti, K., "Large Eddy Simulation of Turbulent Channel Flow by One-Equation Modeling," *Journal of the Physical Society of Japan*, Vol. 54, 1985, pp. 2855-2865.

[7]Hanjalic, K. and Laundar, B.E., "A Reynolds Stress Model of Turbulence and Its Application to Thin Shear Flows," *Journal of Fluid Mechanics*, Vol. 52, 1972, pp. 609-638.

[8]Laundar, B.E., Reece, G.J., and Rodi, W., "Progress in the Development of a Reynolds-Stress Turbulence Closure," *Journal of Fluid Mechanics*, Vol. 68, 1975, pp. 537-566.

[9]Hanjalic, K. and Laundar, B.E., "Contribution towards a Reynolds-Stress Closure for Low-Reynolds-Number Turbulence," *Journal of Fluid Mechanics*, Vol. 74, 1976, pp. 593-610.

[10]Nakao, S., "Contribution to the Reynolds Stress Model as Applied to Near-Wall Region," *AIAA Journal*, Vol. 22, 1984, pp. 303-304.

[11]Bradshaw, P., Cebeci, T., and Whitelaw, J.H., *Engineering Calculation Methods for Turbulent Flow*, Academic, New York, 1981, pp. 37-76.

[12]Demuren, A.O. and Rodi, W., "Calculation of Turbulence-Driven Secondary Motion in Non-Circular Ducts," *Journal of Fluid Mechanics*, Vol. 140, 1984, pp. 189-222.

[13]Patel, V.C., Rodi, W., and Scheuerer, G., "Turbulence Models for Near-Wall and Low Reynolds Number Flows, A Review," *AIAA Journal*, Vol. 23, 1984, pp. 1308-1319.

[14]Jones, W.P. and Launder, B.E., "The Prediction of Laminarization with a Two Equation Model of Turbulence," *International Journal of Heat and Mass Transfer*, Vol. 15, 1972, pp. 301-314.

[15]Jones, W.P. and Launder, B.E., "The Calculation of Low-Reynolds-Number Phenomena with a Two-Equation Model of Turbulence," *International Journal of Heat and Mass Transfer*, Vol. 16, 1973, pp. 1119-1130.

[16]Lam, C.K.G. and Bremhorst, K., "A Modified Form of k-ϵ Model for Predicting Wall Turbulence," *Journal of Fluids Engineering*, Vol. 103, 1981, pp. 456-460.

[17]Chien, K-Y., "Prediction of Channel and Boundary-Layer Flows with a Low-Reynolds-Number Turbulence Model," *AIAA Journal*, Vol. 20, 1982, pp. 33-38.

[18]Kraichnan, R.H., "Direct-Interaction Approximation for Shear and Thermally Driven Turbulence," *The Physics of Fluids*, Vol. 7, 1964, pp. 1048-1062.

[19]Yoshizawa, A, "Statistical Analysis of the Deviation of the Reynolds Stress from Its Eddy-Viscosity Representation," *The Physics of Fluids*, Vol. 27, 1984, pp. 1377-1387.

[20]Yoshizawa, A., "Statistical Theory for Compressible Turbulent Shear Flows, with the Application to Subgrid Modeling," *The Physics of Fluids*, Vol. 29, 1986, pp. 2152-2164.

[21]Laufer, J., "Investigation of Turbulent Flow in a Two-Dimensional Channel," NACA Rept. 1053, 1951.

[22]Clark, J.A., "A Study of Incompressible Turbulent Boundary Layers in Channel Flow," *Transactions of ASME, Journal of Basic Engineering*, Vol. 90, 1968, pp. 455-468.

[23]Kreplin, H. and Eckelmann, M., "Behavior of the Three Fluctuating Velocity Components in the Wall Region of Turbulent Channel Flow," *The Physics of Fluids*, Vol. 22, 1979, pp. 1233-1239.

[24]Robertson, J.M. and Johnson, H.F., "Turbulence Structure in Plane Couette Flow," *Journal of the Engineering Mechanics Division*, ASCE, Vol. 96-EM6, 1970, pp. 1171-1182.

[25]Pai, S.I., "On Turbulent Flow Between Parallel Plates," *Journal of Applied Mechanics*, Vol. 20, 1953, pp. 109-115.

[26]Kobayashi, T. and Kano, M., "Large Eddy Simulation and Numerical Analysis of Turbulent Plane Couette Flow," *Monthly Journal of Institute of Industrial Science*, University of Tokyo, Vol. 38, 1986, pp. 8-14.